Polyhexamethylene Guanidine-induced Lung Injuries and Tumorigenesis in a Rat Model: Radiologic Evaluation With Pathologic Correlation and RNA Sequencing

Cherry Kim
Korea University Ansan Hospital
Sang Hoon Jeong
Korea University Ansan Hospital
Jaeyoung Kim
Korea University Ansan Hospital
Ki Yeol Lee
Korea University Ansan Hospital
Jaehyung Cha
Korea University Ansan Hospital
Chang Hyun Lee
Seoul National University College of Medicine
Eun-Kee Park
Kosin University
Ju-Han Lee (repath@korea.ac.kr)
Korea University College of Medicine and School of Medicine https://orcid.org/0000-0002-5929-5734

Research

Keywords: Chest CT, rat model, Polyhexamethylene guanidine phosphate, RNA sequencing

Posted Date: June 5th, 2020

DOI: https://doi.org/10.21203/rs.3.rs-33203/v1

Abstract

Background: Polyhexamethylene guanidine phosphate (PHMG) is was used as humidifier disinfectants. We aimed to evaluate PHMG-induced lung injuries and their chronological changesin a rat model using chest CT with pathologic correlation, to determine whether PHMG exposure causes lung tumors, and to explore genetic alterations according to PHMG exposure under the guidance of CT.

Methods: A PHMG solution was intratracheally administrated to 40 male rats. Chest CT was carried out in all rats and both lungs were collected for histopathologic evaluation. At 4 weeks after instillation, one lobe of the right lung from 3 rats was subjected to RNA sequencing.

Results: At least one abnormal CT finding was found in all rats at all weeks. The major CT findings were inflammation, fibrosis, and tumors in the pathologic analysis, where significant changes were observed over time.The lung lesions remained persistent after 8 weeks of PHMG exposure. In the pathologic analysis, the extent/severity of inflammation did not show statistically significant changes over time, whereas the extent/severity of fibrosis increased continuously up to 6 weeks after PHMG exposure and then decreased significantly at 8 weeks. Bronchiolar-alveolar adenomas which have malignant potential were found in 50% of rats at 6 and 8 weeks after PHMG exposure. Also, several genes associated with lung cancer, acute lung injury, and pulmonary fibrosis were detected.

Conclusions: PHMG-induced lung injury and its changes according to the number of weeks after exposure were demonstrated using chest CT and pathologic evaluation. In addition, we showed that PHMG exposure caused lung tumors and genetic alterations according toPHMG exposure under the guidance of CT.

Background

Polyhexamethylene guanidine phosphate (PHMG) is a member of the polymeric guanidine family which is widely used as a biocide in the medicine, agriculture, and food industries because of its broad-spectrum antibacterial, antifungal, and antiviral activities in addition to its relatively low toxicity for humans [1]. This compound was used as humidifier disinfectants, and several epidemiological and experimental studies revealed a causal association between PHMG exposure through humidifiers and severe lung injuries [2, 3].

In previous studies, chest CT analysis and pathologic correlations of humidifier disinfectant-associated lung disease were performed in both children and adults [4, 5]. However, in these studies, only patients who had rapidly progressive respiratory distress for several days or weeks were included. Also, the exact length of time and amount of exposure to the humidifier disinfectant and the exact ingredients of humidifier disinfectants were not known due to the retrospective nature of the study design. In addition, lung biopsies were performed in only a few patients and the percentage of patients exposed to humidifier disinfectant which caused lung injury was not investigated. Also, since PHMG is also known to cause cell

cycle arrest and apoptosis in lung epithelial cells [6], we hypothesized that exposure of PHMG may be related to tumorigenesis.

Genomic responses to PHMG exposure using a DNA microarray was investigated, which has been widely used to simultaneously measure the expression levels of a large numbers of genes [7]. This study showed the PHMG changed the expression of genes involved in the urea cycle, inflammation, and oxidative stress in a lung rat model. However, the authors observed changes of the gene expression without knowing any pathologic changes in rat lungs exposed to PHMG. Thus, it is necessary to confirm the presence of pathologic changes in rat lungs using chest CT before performing DNA microarrays.

Therefore, the purposes of this study were to correlate chest CT and pathologic findings of PHMG-induced lung injury in a rat model, to determine whether PHMG exposure causes lung tumors, and to explore genetic alterations according to PHMG exposure under the guidance of CT.

Methods

This study was approved by the Institutional Animal Care and Use Committee of the Korea University Medical Center (Approval number: 2019-0031).

Animals

Nine-week-old male Sprague-Dawley rats (Raonbio, Yong-in, South Korea) were acclimated for 1 week (3 rats per cage) under the following conditions: temperature, 22–25 ℃; relative humidity, 40–60%; and lighting condition, light 12 hours/dark 12 hours. Pelletized food for experimental rodents (Purina, Sung-nam, South Korea) and filtered tap water were given *ad libitum*.

Experimental design

A total of 40 rats were randomly divided into 5 groups. A solution of PHMG was diluted to 0.9 mg/kg with saline using a previously reported method [8]. Then, 50 uL of the PHMG solution was intratracheally administrated to the rats under the guide of a modified videoscope for intratracheal instillation (Additional file 1). At weeks 1, 2, 4, 6, and 8 after instillation (Groups 1 to 5), chest CT examinations of all rats were carried out under anesthesia. Subsequently, the animals were sacrificed and both lungs were collected for histopathologic evaluation. In Group 3, one lobe of the right lung from 3 randomly chosen rats were used for RNA sequencing and the rest of other lobes of these 3 rats were used for histopathologic evaluation. The one lobe in each rat used for RNA sequencing was chosen by one radiologist (C.K.) after reviewing the CT images (lobe with obvious lesions). Lung tissues from control animals (n = 3) were also extracted at 4 weeks after instillation of sterile saline for RNA sequencing. The experimental design is summarized in Fig. 1.

CT protocol

All CT images were scanned using a Philips IQon 128-slice dual-layer detector spectral CT scanner (Philips Healthcare, Cleveland, OH, USA). All images were obtained in a caudo-cranial direction during an inspiration breath-hold using a ventilator for small animals (VentElite, Harvard Apparatus, MA, USA). CT scan parameters were as follows: kVp, 80; mA, 400; collimation, 64 × 0.625 mm; slice thickness, 0.67 mm; beam width, 40 mm; pitch, 1.048; rotation time, 0.4 sec.

CT evaluation

Two board certified radiologists (K.Y.L. and C.K., with 22 and 10 years of experience in thoracic imaging, respectively) who were blinded to the experimental groups and time points reviewed all CT images. Each reviewer evaluated the following CT findings (Fig. 2). The CT findings followed or modified the glossary of radiologic terms suggested by the Fleishner Society [9]. Consolidation was defined as a homogeneous increase in parenchymal attenuation obscuring margins of vessel and airway walls. Hazy increased lung opacity with the preservation of bronchial and vascular margins was defined as GGO. A nodule was defined as a rounded or irregular opacity, well or poorly defined, measuring up to 1 mm in diameter. A well or poorly defined, rounded or irregular opacity over 1 mm was defined as a mass. Centrilobular nodules were nodules which appeared to be separated from the pleural surfaces, fissures, and interlobular septa. Bronchiectasis included bronchial dilatation with respect to the accompanying pulmonary artery, with a lack of tapering of the bronchi. The linear density was a focal or multifocal subsegmental atelectasis showing linear configuration, almost always extending to the pleura.

Among these CT findings, the findings that make up more than two-thirds of the lesions were defined as major CT findings. There were four major CT findings: peribronchial GGO, centrilobular nodules, diffuse GGO, and linear densities and nodules.

The zonal distribution was considered as being the upper lung zone (above the level of the carina), lower lung zone (below the level carina), or whole lung. The prominent location was defined to be ‘posterior’ if there was a predominance of CT findings in the dorsal area and 'peribronchial' if there was predominance along the peribronchovascular area.

Histologic examination

All extracted lung specimens were evaluated by one experienced pathologist with 20 years of clinical experience in lung pathology (J.L.). The lungs were fixed in 10% neutral buffered formalin. From the fixed samples, 4 um thick paraffin sections were cut and hematoxylin and then, eosin (H&E) staining and Masson’s trichrome (MT) staining were performed.

The extent (none, lesions involving < 0–25%/<25–50%/>50% of the total lung areas) and severity (none/mild/moderate/severe) of inflammation and fibrosis were evaluated. The scores of inflammation and fibrosis were calculated by adding the extent and severity of inflammation and fibrosis.

Radiologic-histologic correlation

All major CT findings were compared with matched histologic findings, lesion by lesion, by one radiologist (C.K.) and one pathologist (J.L.), with consensus.

RNA isolation, library preparation/sequencing, and data analysis

Methods for RNA isolation, library preparation/sequencing, and data analysis are described in Additional file 2.

Statistical analysis

The chi-square test for nominal variables and Kruskal–Wallis test for continuous variables were performed to determine differences CT features and pathologic findings among groups, and the chi-square trend analysis for nominal data, Cochran–Mantel–Haenszel test for ordinal data, Jonckheere-Terpstra test for continuous data with Bonferroni corrections were performed for revealing the chronologic changes of CT features and pathologic findings. Inter-observer agreement between two radiologists was assessed with Cohen's kappa statistics. These results were interpreted as follows: < 0.2, poor agreement; 0.21–0.4, fair agreement; 0.41–0.6, moderate agreement; 0.61–0.8, good agreement; > 0.80, very good agreement. All statistical analyses were performed using SPSS Statistics 20 (SPSS, Chicago, IL, USA) or MedCalc version 18.5 (MedCalc Software, Ostend, Belgium). All P-values < 0.05 were considered statistically significant.

Results

CT image analysis

At least one abnormal CT finding was observed in all rats at all weeks. The CT findings according to weeks after PHMG exposure are shown in Table 1. Consolidation was the most frequent at 2 weeks after PHMG exposure with statistically significance (P = 0.012) and then the frequency decreased. GGO was observed in all rats (100%) 1, 4, 6, and 8 weeks after PHMG exposure, and in 7 of 8 rats (87.5%) after 2 weeks. Nodules, masses, and linear densities significantly increased according to the number of weeks after PHMG exposure (all P-values for trend < 0.05).

The major CT findings, zonal predominance, and prominent location of the CT findings according to the number of weeks after PHMG exposure are shown in Table 2 whereas the changes in the major CT findings according to groups are presented in Fig. 3. Peribronchial GGO was observed in all rats 1 week after PHMG exposure and then slightly decreased from 2 to 6 weeks after PHMG exposure before finally disappearing 8 weeks after PHMG exposure. Centrilobular nodules peaked at 4 weeks (37.5%) and then decreased. Linear densities and nodules were observed at 8 weeks (100%). The major CT findings significantly changed according to the number of weeks (P-value for trend < 0.001). Nearly all lung lesions appeared along the peribronchial area in all weeks.

Table 1
CT findings and changes according to the groups.

	After 1 week (Group 1)	After 2 weeks (Group 2)	After 4 weeks (Group 3)	After 6 weeks (Group 4)	After 8 weeks (Group 5)	P-value	P-value for trend
Consolidation	1 (12.5%)	7 (87.5%)	6 (75%)	6 (75%)	3 (37.5%)	0.012	0.767
GGO	8 (100%)	7 (87.5%)	8 (100%)	8 (100%)	8 (100%)	0.395	0.390
Centrilobular nodules	6 (75%)	4 (50%)	7 (87.5%)	4 (50%)	3 (37.5%)	0.229	0.179
Nodule	3 (37.5%)	5 (62.5%)	7 (87.5%)	7 (87.5%)	8 (100%)	0.031	0.003
Mass	0	0	0	1 (12.5%)	2 (25%)	0.217	0.030
Bronchiectasis	0	6 (75%)	8 (100%)	8 (100%)	3 (37.5%)	<0.001	0.166
Linear densities	0	0	4 (50%)	7 (87.5%)	6 (75%)	<0.001	<0.001

GGO, ground glass opacity

Table 2
Major CT findings, zonal predominance, and prominent location of CT findings according to the groups.

	After 1 week (Group 1)	After 2 weeks (Group 2)	After 4 weeks (Group 3)	After 6 weeks (Group 4)	After 8 weeks (Group 5)	P-value	P-value for trend
Major CT findings							
Peribronchial GGO	8 (100%)	6 (75%)	5 (62.5%)	7 (87.5%)	0	<0.001	<0.001
Centrilobular nodules	0	1 (12.5%)	3 (37.5%)	1 (12.5%)	0		
Diffuse GGO	0	1 (12.5%)	0	0	0		
Linear densities and nodules	0	0	0	0	8 (100%)		
Zonal predominance							
Upper (above carina)	0	2 (25%)	0	0	0	0.2	0.2
Lower (below carina)	1 (12.5%)	1 (12.5%)	0	0	1 (12.5%)		
Whole lung	7 (87.5%)	5 (62.5%)	8 (100%)	8 (100%)	7 (87.5%)		
Prominent location							
Posterior	0	1 (12.5%)	0	0	0	0.4	0.4
Peribronchial	8 (100%)	7 (87.5%)	8 (100%)	8 (100%)	8 (100%)		

GGO, ground glass opacity

The two radiologists were in good agreement regarding the presence of CT parameters (Cohen's kappa for GGO, centrilobular nodules, bronchiectasis, and prominent CT features, 1.0; Cohen's kappa for consolidation, 0.955; Cohen's kappa for nodules, 0.945; and Cohen's kappa for mass, 0.877).

Histologic analysis

The changes in the pathologic findings are shown in Table 3 and Fig. 4. Lymphocytic vasculitis was prominent 1 week after PHMG exposure and then decreased (P-value for trend = 0.028). Alveolar hyperplasia peaked at 6 weeks after PHMG exposure and then decreased (P-value for trend = 0.034). Alveolar infiltration of macrophage was observed continuously over all weeks (P-value for trend = 0.884). The presence of foamy histiocytes and lymphoid aggregates peaked at 4 weeks after PHMG exposure

and then decreased (all P-values for trend > 0.05). Tumors were found in 50% of rats at 6 weeks and 50% of rats at 8 weeks after PHMG exposure (all P-values for trend < 0.001). The range of the tumor size was 3 to 8 mm. The tumors were all bronchiolar-alveolar adenomas. The pathologic findings are detailed in Additional file 3.

Table 3
The changes of pathologic findings according to the groups.

	After 1 week (Group 1)	After 2 weeks (Group 2)	After 4 weeks (Group 3)	After 6 weeks (Group 4)	After 8 weeks (Group 5)	P-value	P-value for trend
Major CT findings							
Peribronchial GGO	8 (100%)	6 (75%)	5 (62.5%)	7 (87.5%)	0	< 0.001	< 0.001
Centrilobular nodules	0	1 (12.5%)	3 (37.5%)	1 (12.5%)	0		
Diffuse GGO	0	1 (12.5%)	0	0	0		
Linear densities and nodules	0	0	0	0	8 (100%)		
Zonal predominance							
Upper (above carina)	0	2 (25%)	0	0	0	0.2	0.2
Lower (below carina)	1 (12.5%)	1 (12.5%)	0	0	1 (12.5%)		
Whole lung	7 (87.5%)	5 (62.5%)	8 (100%)	8 (100%)	7 (87.5%)		
Prominent location							
Posterior	0	1 (12.5%)	0	0	0	0.4	0.4
Peribronchial	8 (100%)	7 (87.5%)	8 (100%)	8 (100%)	8 (100%)		

GGO, ground glass opacity

The extent and severity of inflammation and fibrosis are shown in Table 4 and Additional file 4. The extent and severity of inflammation were observed continuously throughout all weeks without statistically significant changes (all P-values for trend > 0.05). There were no significant changes between the weeks in the inflammation scores (P-value for the trend = 0.82). The extent and severity of inflammation and fibrosis gradually increased up to 6 weeks after PHMG exposure and then decreased at

8 weeks (all P-values for trend < 0.05). The fibrosis scores were also significantly greatest at 6 weeks after PHMG exposure and then decreased at 8 weeks (P-value for trend = 0.007).

Table 4
The extent and severity of inflammation and fibrosis according to the groups.

	After 1 week (Group 1)	After 2 weeks (Group 2)	After 4 weeks (Group 3)	After 6 weeks (Group 4)	After 8 weeks (Group 5)	P-value	P-value for trend
Lymphocytic vasculitis							
None	4 (50%)	8 (100%)	7 (87.5%)	7 (87.5%)	8 (100%)	0.057	0.028
Mild	1 (12.5%)	0	0	1 (12.5%)	0		
Moderate	0	0	1 (12.5%)	0	0		
Severe	3 (37.5%)	0	0	0	0		
Alveolar hyperplasia							
None	3 (37.5%)	0	0	0	1 (12.5%)	0.001	0.034
Mild	3 (37.5%)	3 (37.5%)	1 (12.5%)	0	2 (25%)		
Moderate	2 (25%)	4 (50%)	1 (12.5%)	0	4 (50%)		
Severe	0	1 (12.5%)	6 (75%)	8 (100%)	1 (12.5%)		
Alveolar infiltration of macrophage							
None	0	0	0	0	0	0.078	0.884
Mild	3 (37.5%)	2 (25%)	0	0	1 (12.5%)		
Moderate	3 (37.5%)	1 (12.5%)	5 (62.5%)	7 (87.5%)	5 (62.5%)		
Severe	2 (25%)	5 (62.5%)	3 (37.5%)	1 (12.5%)	2 (25%)		
Foamy histiocyte							
None	8 (100%)	0	0	0	2 (25%)	< 0.001	0.058
Mild	0	2 (25%)	0	2 (25%)	1 (12.5%)		
Moderate	0	5 (62.5%)	4 (50%)	5 (62.5%)	5 (62.5%)		
Severe	0	1 (12.5%)	4 (50%)	1 (12.5%)	0		
Lymphoid aggregate							

	After 1 week (Group 1)	After 2 weeks (Group 2)	After 4 weeks (Group 3)	After 6 weeks (Group 4)	After 8 weeks (Group 5)	P-value	P-value for trend
None	3 (37.5%)	1 (12.5%)	1 (12.5%)	4 (50%)	5 (62.5%)	0.016	0.239
Mild	4 (50%)	7 (87.5%)	2 (25%)	1 (12.5%)	3 (37.5%)		
Moderate	0	0	4 (50%)	3 (37.5%)	0		
Severe	1 (12.5%)	0	1 (12.5%)	0	0		
Tumors							
Presence of tumors	0	0	0	4 (50%)	4 (50%)	< 0.001	< 0.001
Number of tumors	0	0	0	1.6 ± 3.1	3.4 ± 8.3	< 0.001	< 0.001
	After 1 week (Group 1)	**After 2 weeks (Group 2)**	**After 4 weeks (Group 3)**	**After 6 weeks (Group 4)**	**After 8 weeks (Group 5)**	**P-value**	**P-value for trend**
Inflammation extent							
None	0	0	0	0	0	0.075	0.932
< 0–25%	4 (50%)	0	0	0	2 (25%)		
< 25–50%	3 (37.5%)	6 (75%)	6 (75%)	6 (75%)	6 (75%)		
> 50%	1 (12.5%)	2 (25%)	2 (25%)	2 (25%)	0		
Inflammation severity							
None	0	0	0	0	0	0.312	0.209
Mild	0	0	0	0	1 (12.5%)		
Moderate	6 (75%)	3 (37.5%)	3 (37.5%)	6 (75%)	5 (62.5%)		
Severe	2 (25%)	5 (62.5%)	5 (62.5%)	2 (25%)	2 (25%)		
Inflammation score	3.88 ± 1.13	4.88 ± 0.84	4.88 ± 0.84	4.50 ± 0.93	3.88 ± 0.99	0.087	0.82
Fibrosis extent							

	After 1 week (Group 1)	After 2 weeks (Group 2)	After 4 weeks (Group 3)	After 6 weeks (Group 4)	After 8 weeks (Group 5)	P-value	P-value for trend
None	5 (62.5%)	2 (25%)	0	0	1 (12.5%)	0.007	0.024
< 0–25%	3 (37.5%)	6 (75%)	6 (75%)	3 (37.5%)	7 (87.5%)		
< 25–50%	0	0	1 (12.5%)	2 (25%)	0		
> 50%	0	0	1 (12.5%)	3 (37.5%)	0		
Fibrosis severity							
None	5 (62.5%)	2 (25%)	0	0	1 (12.5%)	0.014	0.014
Mild	2 (25%)	4 (50%)	5 (62.5%)	1 (12.5%)	4 (50%)		
Moderate	1 (12.5%)	2 (25%)	1 (12.5%)	4 (50%)	3 (37.5%)		
Severe	0	0	2 (25%)	3 (37.5%)	0		
Fibrosis score	0.88 ± 1.25	1.75 ± 1.17	3.00 ± 1.60	4.25 ± 1.58	2.13 ± 0.99	0.002	0.007

Radiologic-histologic correlation

Four major CT findings and the matched major and minor histologic findings are shown in Fig. 5 and Additional file 5. Peribronchial GGO was observed in 26 rats (65%) in all groups, and was matched with the infiltrate of histiocytes (84.6%) and fibrosis in peribronchial and/or alveolar spaces (15.4%). Centrilobular nodules were found in 5 rats in all groups (12.5%) in addition to matched fibrosis in peribronchial and/or alveolar spaces (60%) and the infiltrate of histiocytes and lymphocytes in the peribronchial/alveolar space (40%). Linear densities and nodules were major findings of 8 rats (20%) in Group 5. The matched major pathologic findings were the infiltrate of histiocytes and lymphocytes in peribronchial/alveolar spaces (62.5%), fibrosis in peribronchial/alveolar spaces (25%), and bronchiolo-alveolar adenomas (12.5%). Diffuse GGO was found in one rat in Group 2 and the matched histologic finding was the infiltrate of histiocytes in the alveolar spaces.

RNA sequencing analysis

A total of 96 genes among 17,048 genes significantly expressed changes in PHMG-instillated lung tissue with a standard P-value < 0.05 and log > 2 or <-2. Among these, 64 genes were upregulated and 32 genes were downregulated compared to lung tissues of wild-type rat (Fig. 6). Additional file 6 summarizes these 96 significantly upregulated or downregulated genes. Among the PHMG-regulated genes, *CXCR1*, *AQP3*,

ROR2, *IQGAP3*, *SUV39H2*, and *THBS2* are upregulated [10–15], and *RSPO1*, *WNT2B*, *CALML3*, *GATA4*, *CES1C*, *BMP7*, *SPRY2*, and *TNFRSF25* are downregulated [16–20], which are associated with lung cancer. In addition, there were some upregulated genes which have been implicated in mediating pulmonary disorders, such as ALOX15, which induces acute lung injury [21], and *PDE1A*, *CHI3L1*, and *BPIFB1*, which play a critical role in pulmonary fibrosis [22–24]. In addition, there were no genes associated with DNA repair and RNA splicing, and the genes related to cell proliferation were significantly downregulated (Additional file 7).

Discussion

In this study, we evaluated PHMG-induced lung injury and its changes according to the number of weeks after exposure in a rat model using chest CT and pathologic evaluation. In addition, we proved that PHMG exposure caused lung tumors and genetic alterations under the guidance of CT.

In both the chest CT and pathologic analyses, at least one lesion in the lung appeared every week in all rats exposed to PHMG, despite the single exposure. In addition, the major CT findings of lung lesions showed significant changes over time, which were also proved though pathologic evaluation, and the lung lesions remained persistent after 8 weeks of exposure. In the pathologic analysis, the extent and severity of inflammation did not show statistically significant changes over time, whereas the extent and severity of fibrosis increased continuously up to 6 weeks after exposure and then decreased significantly at 8 weeks. Among the major CT findings, we found that 84.6% of peribronchial GGOs were inflammation and the rest were fibrosis through a radiologic-histologic correlation. Centrilobular nodules were 60% fibrosis and the rest were inflammation, the linear densities and nodules were 62.5% inflammation, 25% fibrosis, and 12.5% tumors, and diffuse GGO was inflammation (100%). Most of the lesions were located along the peribronchial area, which may be due to the fact that PHMG was instilled through the trachea and reacted by spreading along the bronchus. These findings suggest that PHMG can cause significant lung injury and if exposed to PHMG, the lesion can be evaluated by chest CT. In previous studies, exudates fill the alveolar air space as well as the peribronchial fibro-inflammatory lesions in both early and chronic stages in pediatric patients [25]. In adult patients, extensive fibrosis was also noted in the chronic stage [5]. However, in the previous study, they did not analyze pathologic findings which correlated with CT findings in all patients. Several studies using mice also reported severe pulmonary inflammation and fibrosis caused by PHMG exposure [8, 26]. PHMG exposure led to persistent pulmonary inflammation and fibrosis for at least 10 weeks and dose-dependent exacerbation of both inflammation and pulmonary fibrosis on day 14 was found. However, these studies did not provide quantitative pathologic finding results and did not analyze the changes of pathologic findings over time in detail. In addition, there have been no studies on the occurrence of lung lesions and changes according to time caused by PHMG using chest CT.

Another important finding in our study is the incidence of tumors caused by PHMG. Previous studies have not reported the incidence of tumors, probably because the pathologic evaluation did not include the section where the tumor grew. In this study, the CT findings were analyzed in advance and slides were

made in consideration of the mass or nodule part. As a result, we found tumors in 50% of rats 6 and 8 weeks after exposure. In addition, our study was the first to detect tumors in lungs exposed to PHMG.

In our study, the tumors were all bronchiolar-alveolar adenomas. A spectrum of bronchiolar-alveolar proliferative lesions such as hyperplasia-adenoma-adenocarcinoma has been best described in rodents, where they can occur after exposure of various carcinogens or spontaneously [27]. Bronchiolar-alveolar proliferative lesions apparently represent a spectrum that progresses from hyperplasia to adenoma to carcinoma in rodents and some researchers have argued that all lesions should be designated as carcinomas, even in earliest lesions. In addition, bronchioloalveolar neoplasms in human are generally considered malignant [27]. In our study, analysis was only performed up to 8 weeks after PHMG exposure, but considering the spectrum of bronchiolar-alveolar proliferation, the possibility of carcinoma being discovered after 8 weeks cannot be excluded. Therefore, in future work, it is important to consider results beyond 8 weeks.

In the RNA sequencing analysis, we found several genes associated with lung cancer, acute lung injury, and pulmonary fibrosis. In addition, there were no genes associated with DNA repair and RNA splicing, and the genes related to cell proliferation were significantly downregulated. Since the lung lobes with lesions were identified using CT beforehand, the tissues to be used for RNA sequencing were selected, resulting in a more robust and direct gene association with the lung lesions. It has been reported that dysregulation of DNA repair and RNA splicing can cause various genetic disorders and eventually lead to cancer [28–30]. Taken together, our results demonstrate that genetic alterations due to PHMG exposure may provoke pulmonary inflammation and pulmonary fibrosis by attenuating the normal recovery mechanism of the lung, consequently resulting in tumorigenesis.

There were several limitations in this study. First, RNA sequencing was performed for only three rats at 4 weeks after PHMG exposure. However, because the primary goal of this study was CT imaging analysis with pathologic correlation, much of the tissue could not be utilized for RNA sequencing. In addition, since the tumors were detected 6 weeks after exposure, gene analysis may be necessary in rats after 6 weeks. Second, it is difficult to accurately correlate the dose instilled in rats with the amount of inhalation through the humidifier in humans. In addition, further studies are needed to determine the extent and severity of lung lesions, including tumors, using a smaller or higher dose in addition to the concentrations used in this experiment.

Conclusions

In conclusion, at least one lesion in the lung appeared every week in all rats exposed to PHMG in chest CT and pathologic analyses, despite the single exposure. In addition, the major CT findings of lung lesions showed significant changes over time, which were also verified though pathologic evaluation, and the lung lesions remained persistent after 8 weeks of exposure. We found bronchiolar-alveolar adenomas, which have malignant potential, in 50% of rats 6 and 8 weeks after exposure. Also, several genes associated with lung cancer, acute lung injury, and pulmonary fibrosis were found. The genetic alterations

due to PHMG exposure may provoke pulmonary inflammation and pulmonary fibrosis by attenuating the normal recovery mechanism of the lung and consequently result in tumorigenesis.

Abbreviations

PHMG
Polyhexamethylene guanidine phosphate
GGO
ground-glass opacity

Declarations

Ethics approval and consent to participate

This study was approved by the Institutional Animal Care and Use Committee of the Korea University Medical Center (Approval number: 2019-0031).

Consent for publication

Not applicable.

Availability of data and materials

Not applicable.

Competing interests

The authors declare that they have no competing interests.

Funding

This study was supported by the Korea Ministry of Environment (2018001360002), National Research Foundation of Korea (NRF-2018R1D1A1B07049989), Korea university Ansan hospital research grant (O1903581), and Korea university grant (K2008271).

Authors' contributions

Conception and design: C.K., S.H.J., J.K., J.L.; acquisition of data: C.K., S.H.J., J.K., J.L.; analysis and interpretation of data: all authors; drafting the article or revising it critically for important intellectual content: C.K., S.H.J., J.K., J.L; final approval of the version to be published: all authors.

References

1. Park YJ, Jeong MH, Bang IJ, Kim HR, Chung KH. **Guanidine-based disinfectants, polyhexamethylene guanidine-phosphate (PHMG-P), polyhexamethylene biguanide (PHMB), and oligo(2-(2-ethoxy)ethoxyethyl guanidinium chloride (PGH) induced epithelial-mesenchymal transition in A549 alveolar epithelial cells**. *Inhal Toxicol* 2019:1–6.
2. Lee MS, Kim HJ. Epidemiologic research on lung damage caused by humidifier disinfectants. Epidemiol Health. 2016;38:e2016031.
3. Park JH, Kim HJ, Kwon GY, Gwack J, Park YJ, Youn SK, Kwon JW, Yang BG, Lee MS, Jung M, et al. Humidifier Disinfectants Are a Cause of Lung Injury among Adults in South Korea: A Community-Based Case-Control Study. PLoS One. 2016;11:e0151849.
4. Yoon J, Cho HJ, Lee E, Choi YJ, Kim YH, Lee JL, Lee YJ, Hong SJ. Rate of humidifier and humidifier disinfectant usage in Korean children: A nationwide epidemiologic study. Environ Res. 2017;155:60–3.
5. Koo HJ, Do KH, Chae EJ, Kim HJ, Song JS, Jang SJ, Hong SB, Huh JW, Lee E, Hong SJ. Humidifier disinfectant-associated lung injury in adults: Prognostic factors in predicting short-term outcome. Eur Radiol. 2017;27:203–11.
6. Park JS, Park YJ, Kim HR, Chung KH. Polyhexamethylene guanidine phosphate-induced ROS-mediated DNA damage caused cell cycle arrest and apoptosis in lung epithelial cells. J Toxicol Sci. 2019;44:415–24.
7. Kim MS, Jeong SW, Choi SJ, Han JY, Kim SH, Yoon S, Oh JH, Lee K. Analysis of genomic responses in a rat lung model treated with a humidifier sterilizer containing polyhexamethyleneguanidine phosphate. Toxicol Lett. 2017;268:36–43.
8. Song J, Kim W, Kim YB, Kim B, Lee K. Time course of polyhexamethyleneguanidine phosphate-induced lung inflammation and fibrosis in mice. Toxicol Appl Pharmacol. 2018;345:94–102.
9. Hansell DM, Bankier AA, MacMahon H, McLoud TC, Muller NL, Remy J. Fleischner Society: glossary of terms for thoracic imaging. Radiology. 2008;246:697–722.
10. Khan MN, Wang B, Wei J, Zhang Y, Li Q, Luan X, Cheng J-W, Gordon JR, Li F, Liu HJO. **CXCR1/2 antagonism with CXCL8/interleukin-8 analogue CXCL8 (3–72) K11R/G31P restricts lung cancer growth by inhibiting tumor cell proliferation and suppressing angiogenesis**. 2015, 6:21315.
11. Liu YL, Matsuzaki T, Nakazawa T, Murata S-i, Nakamura N, Kondo T, Iwashina M, Mochizuki K, Yamane T. Takata KJHp: **Expression of aquaporin 3 (AQP3) in normal and neoplastic lung tissues**. 2007, 38:171–178.
12. Lu C, Wang X, Zhu H, Feng J, Ni S, Huang JJO. **Over-expression of ROR2 and Wnt5a cooperatively correlates with unfavorable prognosis in patients with non-small cell lung cancer**. 2015, 6:24912.
13. Yang Y, Zhao W, Xu Q-W, Wang X-S, Zhang Y, Zhang JJPo. **IQGAP3 promotes EGFR-ERK signaling and the growth and metastasis of lung cancer cells**. 2014, 9:e97578.
14. Zheng Y, Li B, Wang J, Xiong Y, Wang K, Qi Y, Sun H, Wu L, Yang LJCe: **Identification of SUV39H2 as a potential oncogene in lung adenocarcinoma**. 2018, **10**:129.

15. Weng T-Y, Wang C-Y, Hung Y-H, Chen W-C, Chen Y-L, Lai M-DJPo: **Differential expression pattern of THBS1 and THBS2 in lung cancer: clinical outcome and a systematic-analysis of microarray databases**. 2016, **11**:e0161007.
16. Wu L, Zhang W, Qian J, Wu J, Jiang L, Ling CJOL. **R–spondin family members as novel biomarkers and prognostic factors in lung cancer**. 2019, 18:4008–4015.
17. Zhan C, Yan L, Wang L, Sun Y, Wang X, Lin Z, Zhang Y, Shi Y, Jiang W, Wang QJJotd. **Identification of immunohistochemical markers for distinguishing lung adenocarcinoma from squamous cell carcinoma**. 2015, 7:1398.
18. Gao L, Hu Y, Tian Y, Fan Z, Wang K, Li H, Zhou Q, Zeng G, Hu X, Yu LJNc. **Lung cancer deficient in the tumor suppressor GATA4 is sensitive to TGFBR1 inhibition**. 2019, 10:1665.
19. Chen J, Ye L, Xie F, Yang Y, Zhang L, Jiang WGJAr. **Expression of bone morphogenetic protein 7 in lung cancer and its biological impact on lung cancer cells**. 2010, 30:1113–1120.
20. Schreiber TH, Wolf D, Tsai MS, Chirinos J, Deyev VV, Gonzalez L, Malek TR, Levy RB. Podack ERJTJoci: **Therapeutic Treg expansion in mice by TNFRSF25 prevents allergic lung inflammation**. 2010, 120:3629–3640.
21. Rossaint J, Nadler JL, Ley K, Zarbock AJCC. **Eliminating or blocking 12/15-lipoxygenase reduces neutrophil recruitment in mouse models of acute lung injury**. 2012, 16:R166.
22. Ren L, Yang C, Dou Y, Zhan R, Sun Y, Yu YJElr: **MiR-541-5p regulates lung fibrosis by targeting cyclic nucleotide phosphodiesterase 1A**. 2017, **43**:249–258.
23. Zhou Y, Peng H, Sun H, Peng X, Tang C, Gan Y, Chen X, Mathur A, Hu B. Slade MDJStm: **Chitinase 3–like 1 suppresses injury and promotes fibroproliferative responses in mammalian lung fibrosis**. 2014, 6:240ra276-240ra276.
24. Bingle L, Wilson K, Musa M, Araujo B, Rassl D, Wallace WA, LeClair EE, Mauad T, Zhou Z. Mall MAJH, biology c: **BPIFB1 (LPLUNC1) is upregulated in cystic fibrosis lung disease**. 2012, 138:749–758.
25. Yoon HM, Lee E, Lee JS, Do KH, Jung AY, Yoon CH, Kim SO, Jang SJ, Hong SJ, Cho YA. Humidifier disinfectant-associated children's interstitial lung disease: Computed tomographic features, histopathologic correlation and comparison between survivors and non-survivors. Eur Radiol. 2016;26:235–43.
26. Kim HR, Lee K, Park CW, Song JA, Shin DY, Park YJ, Chung KH. Polyhexamethylene guanidine phosphate aerosol particles induce pulmonary inflammatory and fibrotic responses. Arch Toxicol. 2016;90:617–32.
27. Miller GF. Bronchiolar-alveolar adenoma in a rhesus monkey (Macaca mulatta). Vet Pathol. 1994;31:388–90.
28. Doukas SG, Vageli DP, Nikolouzakis TK, Falzone L, Docea AO, Lazopoulos G, Kalbakis K. Tsatsakis AJWAoSJ: **Role of DNA mismatch repair genes in lung and head and neck cancer**. 2019, 1:184–191.
29. Landi S, Gemignani F, Canzian F, Gaborieau V, Barale R, Landi D, Szeszenia-Dabrowska N, Zaridze D, Lissowska J. Rudnai PJCr: **DNA repair and cell cycle control genes and the risk of young-onset lung cancer**. 2006, 66:11062–11069.

30. Scotti MM, Swanson MSJNRG. **RNA mis-splicing in disease**. 2016, 17:19.

Figures

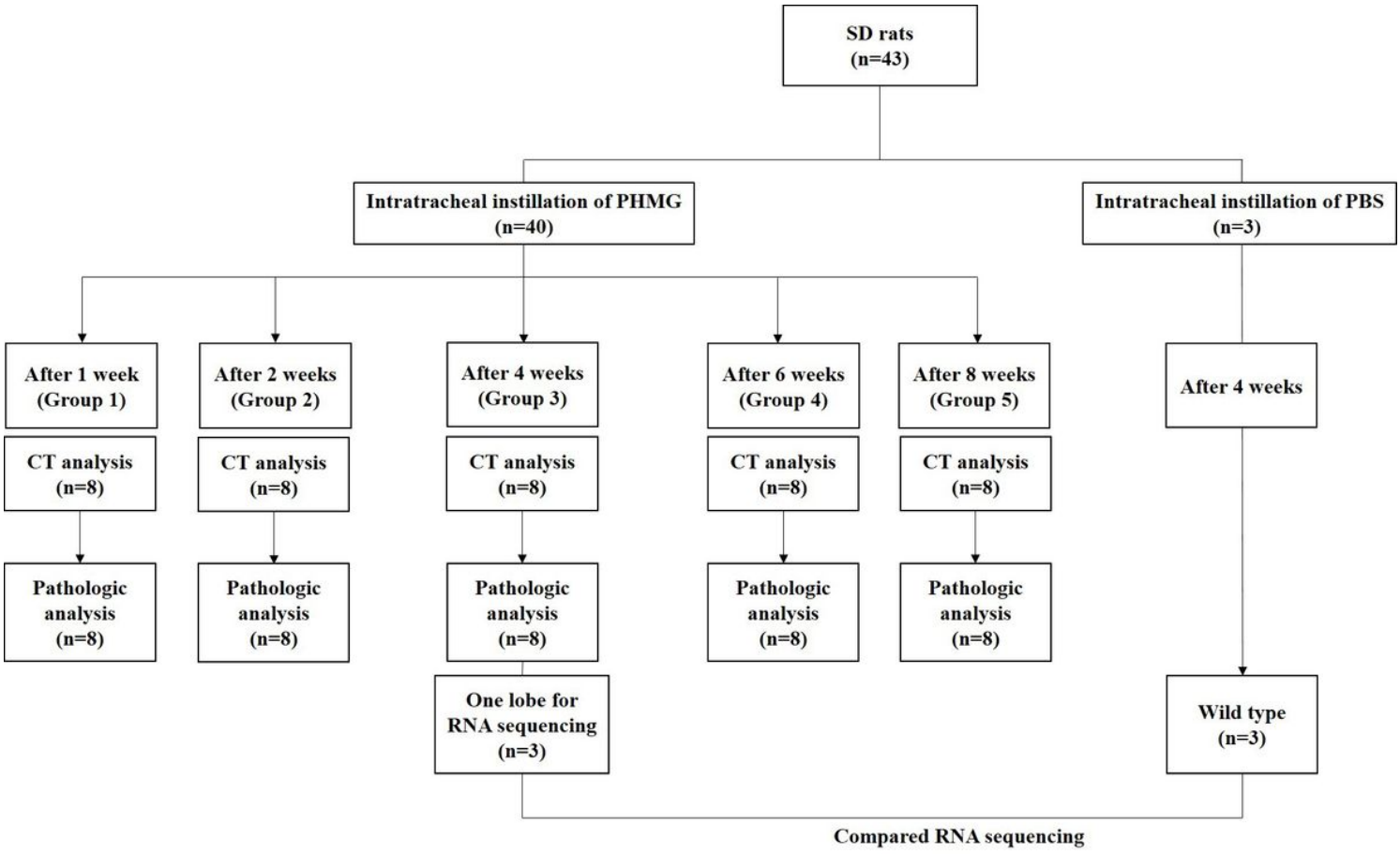

Figure 1

The experimental design. 1, 2, 4, 6, and 8 weeks after instillation (Groups 1 to 5), chest CT examination was conducted in all rats under anesthesia. Subsequently, the animals were sacrificed and both lungs were collected for histopathologic evaluation. In Group 3 (4 weeks after instillation), one lobe of the right lung from 3 randomly chosen rats were used for RNA sequencing and the other lobes of those 3 rats were used for histopathologic evaluation. The lung tissue from control animals (n=3) was also extracted 4 weeks after the instillation of sterile saline instead of PHMG for RNA sequencing.

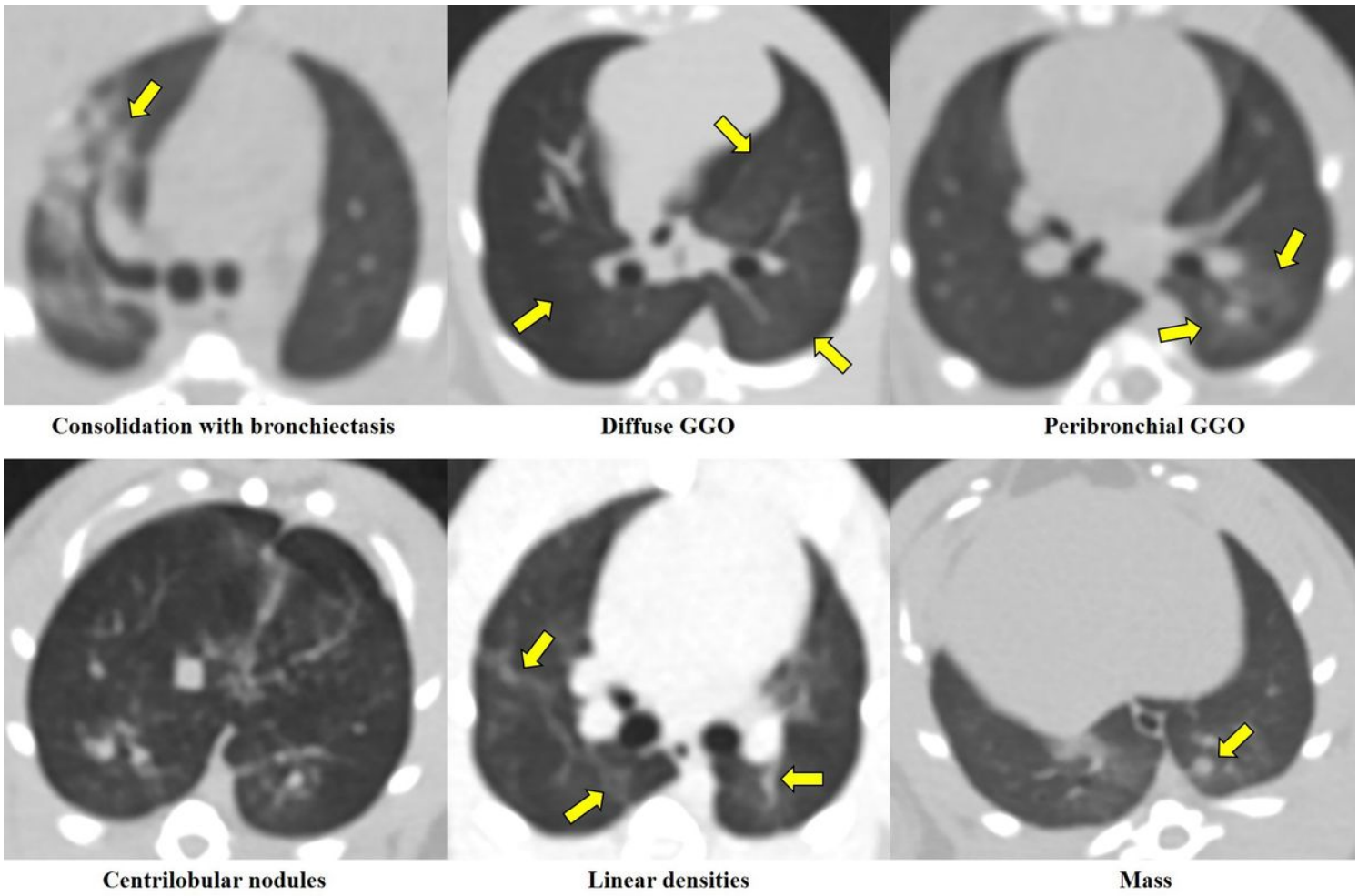

Figure 2

Examples of CT findings. Consolidation, ground-glass opacity (GGO), nodules, masses, centrilobular nodules, bronchiectasis, and linear atelectasis were followed or modified the glossary of radiologic terms suggested by the Fleishner Society.

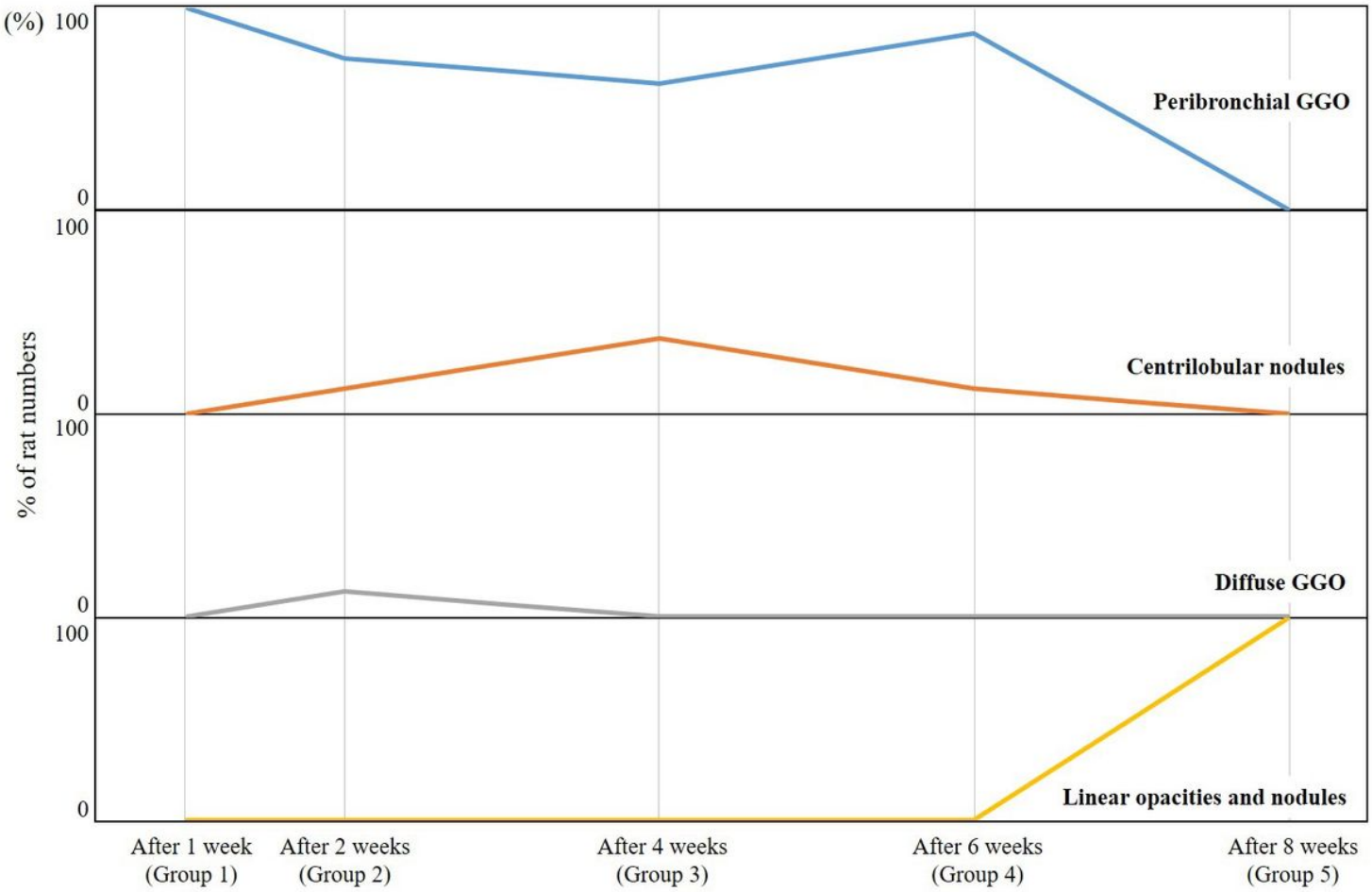

Figure 3

Changes of the CT findings according to the groups. Peribronchial GGO was observed in all rats 1 week after PHMG exposure, then slightly decreased through 2 weeks to 6 weeks after PHMG exposure, and disappeared at 8 weeks after PHMG exposure. Centrilobular nodules peaked at 4 weeks (3 of 8 rats, 37.5%) and then decreased. Linear densities and nodules were observed at 8 weeks (8 of 8 rats, 100%).

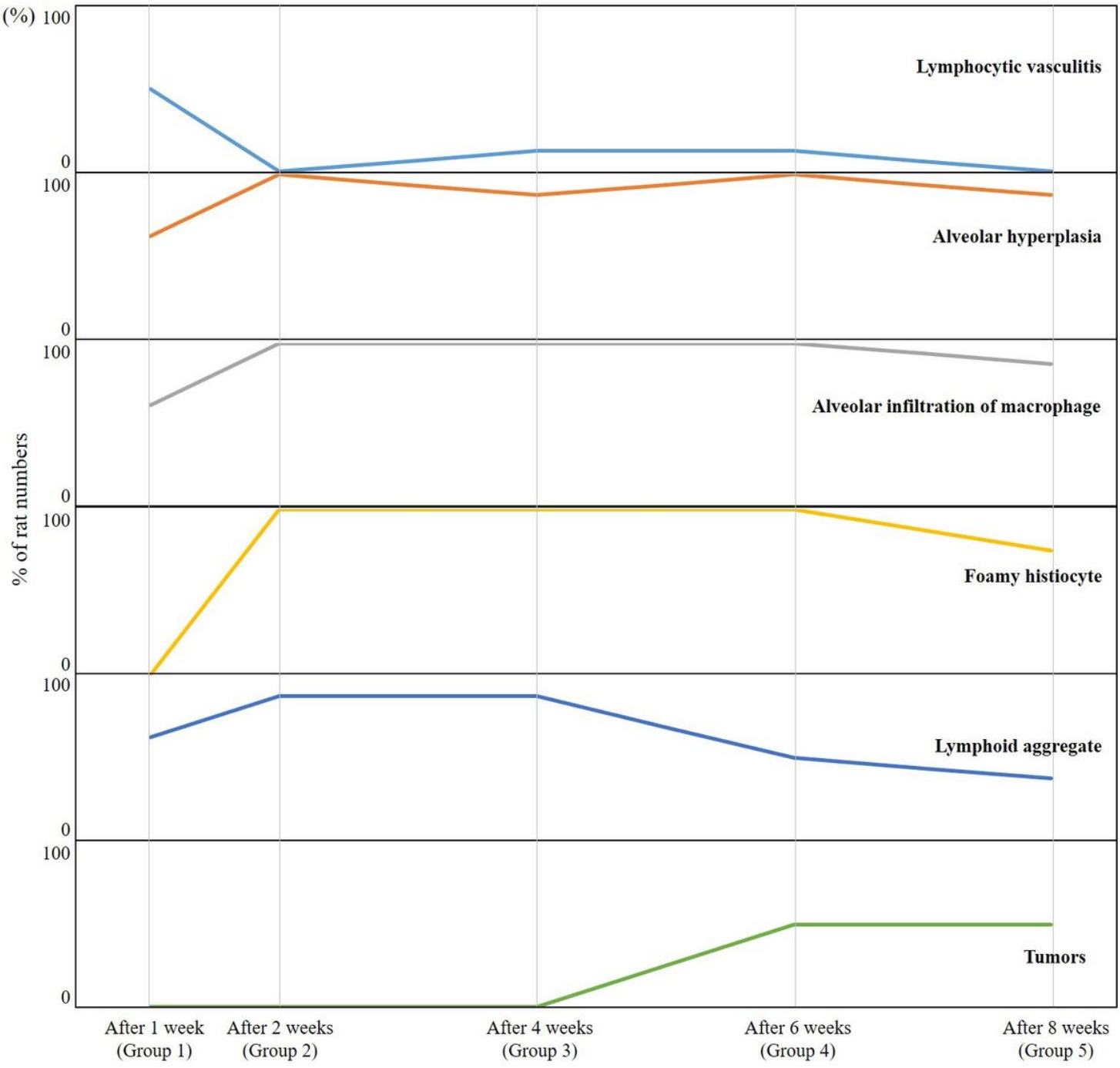

Figure 4

Changes in the pathologic findings according to group.Lymphocytic vasculitis was prominent 1 week after PHMG exposure and then decreased (P=0.057, P-value for trend=0.028). Alveolar hyperplasia peaked at 6 weeks after PHMG exposure and then decreased (P=0.001, P-value for trend=0.034). Alveolar infiltration of macrophages was observed continuously over all weeks (P=0.078, P-value for trend=0.884). Foamy histiocyte and lymphoid aggregate peaked at 4 weeks after PHMG exposure and then decreased (all P<0.05, all P-value for trend >0.05). Tumors were found in 50% of rats (4 of 8 rats) at 6 weeks and 50% of rats (4 of 8 rats) at 8 weeks after PHMG exposure (all P<0.001, all P-value for trend <0.001).

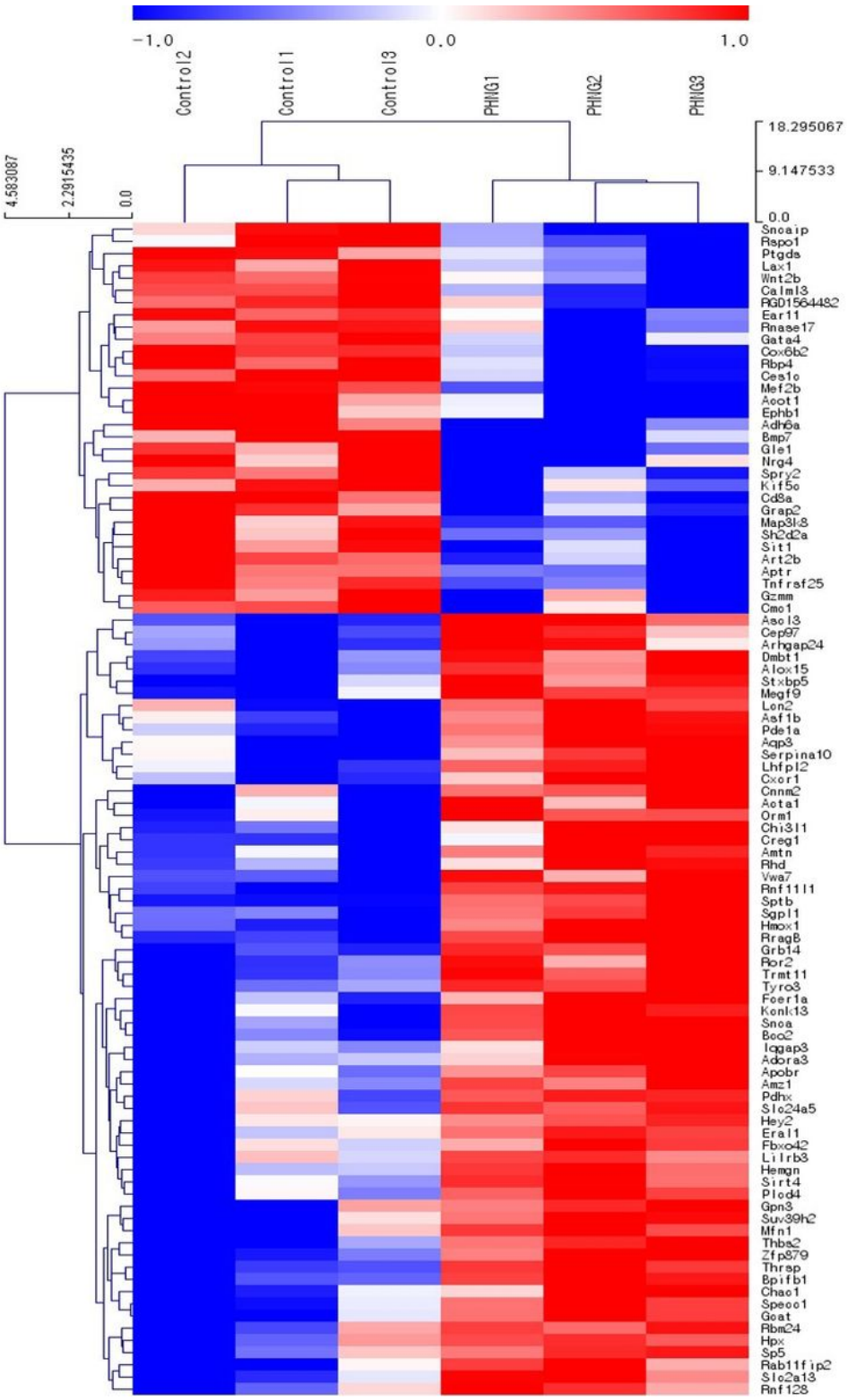

Figure 5

Four major CT findings and matched major histologic findings. Through radiologic-histologic correlation, 84.6% of peribronchial GGOs were inflammation and the rest were fibrosis. Centrilobular nodules were 60% fibrosis and the rest were inflammation, linear densities and nodules were 62.5% inflammation, 25% fibrosis, and 12.5% tumors, and diffuse GGO was inflammation (100%).

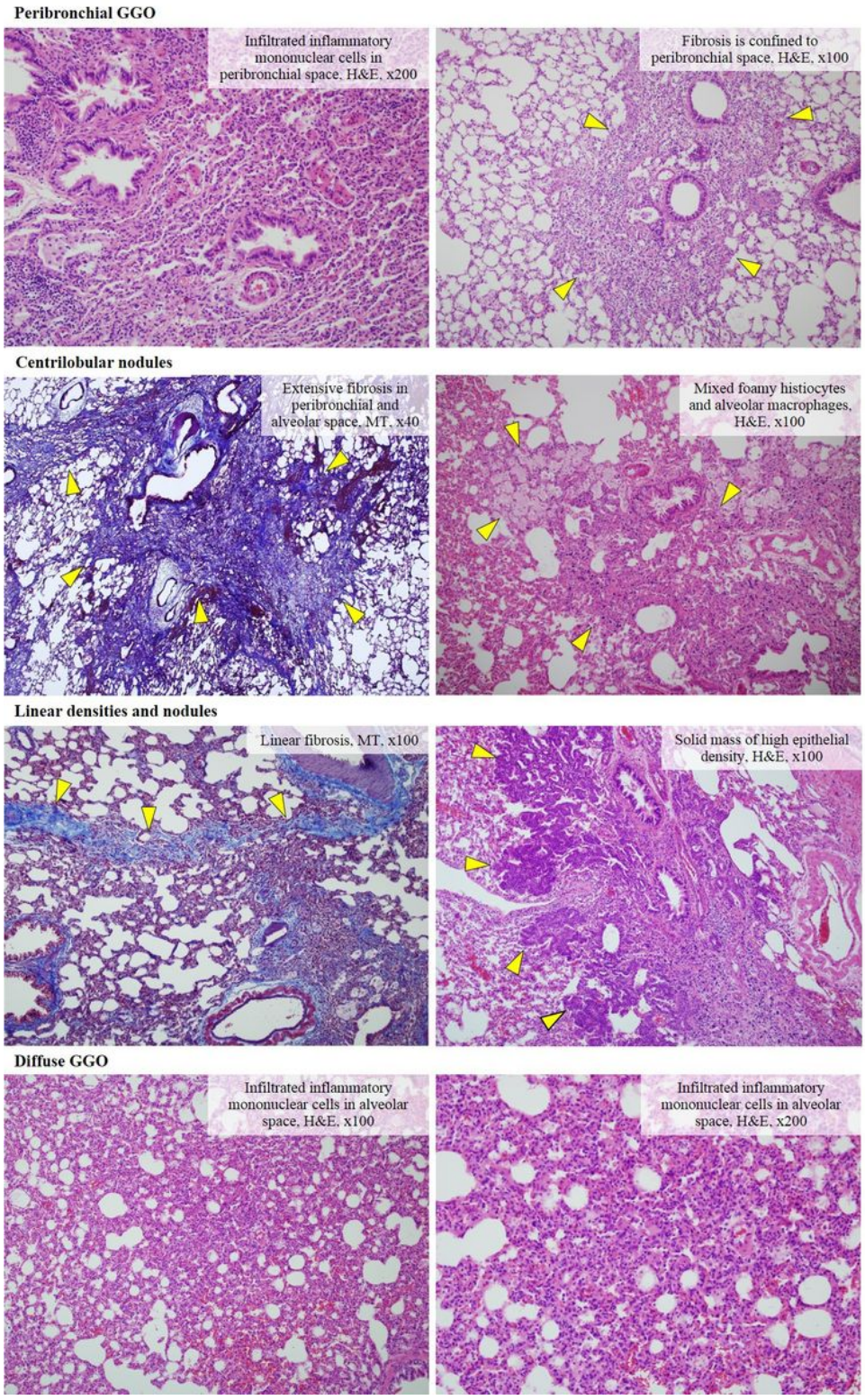

Figure 6

Analysis of PHMG-regulated gene expression in rat lung tissue. Heatmap of PHMG regulated genes (>2-fold, $p<0.05$) based on gene clustering of QuantSeq 3’ mRNA-Seq results.

Supplementary Files

This is a list of supplementary files associated with this preprint. Click to download.

- Additionalfile2.docx
- Additionalfile5.docx
- Additionalfile4.docx
- Additionalfile1.docx
- Additionalfile3.docx
- Additionalfile6.docx
- Additionalfile7.docx